electronics

MDPI

Article

Design and Parameter Optimization of Double-Mosquito Combination Coils for Enhanced Anti-Misalignment Capability in Inductive Wireless Power Transfer Systems

Wencong Huang *, Jinying Huang, Ying Hu, Yuqiao Zhu and Yufang Chang

Faculty of Electric and Electrical Engineering, Hubei University of Technology, Wuhan 430070, China; 102110313@hbut.edu.cn (J.H.); 102110361@hbut.edu.cn (Y.H.); 102110346@hbut.edu.cn (Y.Z.); changyf@hbut.edu.cn (Y.C.)

* Correspondence: hwc@hbut.edu.cn; Tel.: +86-13554210167

Abstract: This paper proposes a novel double-mosquito combination (DMC) coil for inductive wireless power transfer (IPT) systems to improve their anti-misalignment capability. The DMC coil consists of a mosquito coil with single-turn spacing and a tightly wound close-wound coil. By superimposing the magnetic fields generated by both coils, a relatively uniform magnetic field distribution is achieved on the receiving coil plane. This approach addresses the challenges of significant output voltage fluctuations and reduced transmission efficiencies caused by coupling coil misalignments in conventional IPT systems. To further optimize the DMC coil, an interaction law between its parameters and the mutual inductance is established, setting the coil mutual inductance fluctuation rate as the optimization objective, and using the coil turn spacing, number of turns, and outer diameter as constraint conditions. The beetle antennae search algorithm (BAS) is employed to enhance the whale optimization algorithm (WOA), facilitating the adaptive optimization of the coil parameters. An experimental IPT system platform with a 50 mm transmission distance is developed to validate the robust anti-misalignment capability of the proposed coil. The results demonstrate that within a horizontal misalignment range of 50 mm, the system's output voltage fluctuation rate stays below 7.4%, and the transmission efficiency remains above 83%.

Keywords: inductive wireless power transfer; double-mosquito combination coil; improved whale optimization algorithm; parameter optimization; anti-misalignment capability

check for updates

Citation: Huang, W.; Huang, J.; Hu, Y.; Zhu, Y.; Chang, Y. Design and Parameter Optimization of Double-Mosquito Combination Coils for Enhanced Anti-Misalignment Capability in Inductive Wireless Power Transfer Systems. *Electronics* **2024**, *13*, 838. https://doi.org/10.3390/electronics13050838

Academic Editor: Niamat Hussain

Received: 17 January 2024
Revised: 10 February 2024
Accepted: 19 February 2024
Published: 21 February 2024

Copyright: © 2024 by the authors. Licensee MDPI, Basel, Switzerland. This article is an open access article distributed under the terms and conditions of the Creative Commons Attribution (CC BY) license (https://creativecommons.org/licenses/by/4.0/).

1. Introduction

Grounded in the principles of electromagnetic induction, the inductive wireless power transfer (IPT) technology facilitates wireless power transfer by establishing electromagnetic coupling between transmitting and receiving coils [1–3]. This innovative technology offers numerous benefits such as safety, flexibility, and convenience, making it a promising solution for a wide range of applications. These applications include electric vehicles [4], underwater operations [5], automatic guided vehicles (AGVs) [6,7], and implantable medical devices [8].

The AGV, a handling tool that follows a set path, can significantly cut labor costs, boost productivity, and is commonly employed in various industries, transportation, and other sectors. The use of IPT systems to transfer power to AGVs in real-world scenarios inevitably results in vehicular vibrations during operation, causing the position of the receiving coil, mounted on the vehicle chassis, to shift in relation to the stationary transmitting coil embedded in the road surface. This displacement leads to changes in the IPT system's mutual inductance [9], affecting both the output power and transmission efficiency. Consequently, it is crucial to prioritize the investigation of the coil structure design and parameter optimization for the coupling mechanism in order to enhance the IPT system's anti-misalignment performance [10,11].

Enhancing the anti-misalignment capabilities of IPT systems through coil structure design hinges on the construction of a uniform magnetic field [12]. A transmitting coil with a uniform magnetic field distribution enables the receiving coil to be positioned freely, maintaining the stability of the output power and transmission efficiency. Numerous transmitting coil design methods have been proposed by researchers worldwide to achieve a uniform magnetic field distribution. The literature [13] employs partial magnetic field cancellation and introduces a transmitting coil structure that combines forward and reverse winding, resulting in a uniform longitudinal magnetic field intensity distribution on the receiving coil plane. The literature [14] minimizes the mutual inductance fluctuation rate within the misalignment range by connecting a reverse-wound coil in series at the transmitting end. However, both [13,14] rely on the enumeration method, which entails lengthy simulation calculations and complex optimization processes.

The literature [15] suggests a group series winding–transmitting coil structure that involves winding two close-wound coil groups in series. This design achieves a uniform transverse magnetic flux generated by the transmitting coil when its outer diameter is larger than that of the receiving coil, but it only considers a single close-wound coil combination. The literature [16] proposes a combined series winding hexagonal coil structure that merges tightly and loosely wound coils. Although this approach improves the coupling coefficients and anti-misalignment abilities of wireless power transfer systems, it merely combines mosquito and close-wound coils without further examining the impact of different turn-spacing coil arrangement methods on the coil's magnetic induction intensity distribution. Furthermore, it does not consider the optimal combination method for achieving the most uniform magnetic field distribution.

This paper aims to achieve a relatively uniform magnetic field distribution by combining close-wound and mosquito coils and determining the best combination method through a comparison of the coils' magnetic induction intensity distributions generated under various arrangement methods. In addition, to minimize mutual inductance fluctuations during the coupling coil misalignment process and to enhance the output power and transmission efficiency, the paper incorporates the tentacle algorithm to improve the whale algorithm, thus deriving the optimal coil turn spacing and the number of turns under given constraint conditions. The main contributions of this paper are listed as follows:

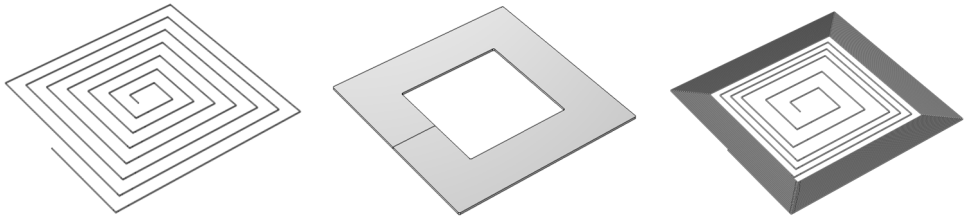
(1) A proposed double-mosquito combination (DMC) coil structure combines the magnetic induction intensity distribution analysis of the mosquito coil and the close-wound coil. This coil exhibits a relatively uniform magnetic field distribution, which can reduce the mutual inductance and output voltage fluctuation rate of the IPT system after deviation.
(2) The integration of the beetle antennae search algorithm into the whale algorithm is presented to calculate the novel optimal whale position using the position update formula of the beetle antennae search algorithm. Compared with the optimal whale position calculated by the conventional whale algorithm, the smaller one is selected as the optimal position within the current whale population, thereby further enhancing the convergence speed and accuracy of the whale algorithm.
(3) With the minimization of the coil's mutual inductance fluctuation rate as the optimization target, the parameters of the DMC coil are optimized using the improved whale algorithm, which enhances the resistance to misalignment of the DMC coil and ensures the efficient and stable operation of the IPT system.

The rest of the paper is organized as follows: Section 2 presents an equivalent circuit diagram of the IPT system, combining the coil, and establishes the relationships among system output power, transmission efficiency, and mutual inductance. In Section 3, the magnetic field distribution of the mosquito and close-wound coils is obtained through simulation. A model of two single-turn square coils coaxially aligned is developed, and the interaction law between the coil parameters and mutual inductance of transmitting and receiving coils is analyzed. Section 4 details the DMC coil design method, optimizes the DMC coil parameters using a specific algorithm, and examines the misalignment characteristics of

the optimized DMC coil. Section 5 describes the construction of an experimental platform for the IPT system, providing verification of the robust anti-misalignment capability of the DMC coil after parameter optimization within a horizontal misalignment range of ±50 mm at a transmission distance of 50 mm. Finally, Section 6 concludes the paper.

2. Transmission Characteristics Analysis of IPT System with Combined Coils

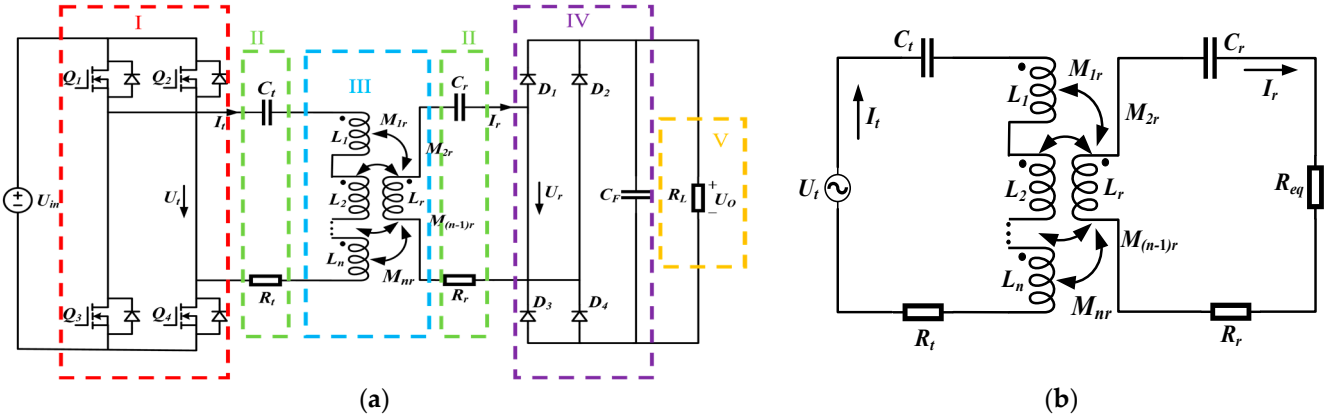
At present, there are mainly two types of traditional planar square coils: mosquito coils with single-turn spacing and close-wound coils with tight winding. Figure 1 illustrates the comparison between the combined coil suggested in this study and the conventional square coil structure.



(**a**) (**b**) (**c**)

Figure 1. Structure comparison between traditional square coil and combined coil: (**a**) mosquito coil; (**b**) close-wound coil; and (**c**) combined coil.

The combined coil integrates the winding features of both the mosquito coil and the close-wound coil, resulting in a coil with varying turn spacings from the inner to the outer section using a single wire. Based on its winding characteristics, the circuit diagram for the IPT system is illustrated in Figure 2. The IPT system primarily consists of a high-frequency inverter (I), compensation network (II), magnetic coupling mechanism (III), rectifier filter circuit (IV), and load (V) [17,18]. Furthermore, the system employs a straightforward structure and a more stable power factor series–series (SS) compensation network.



(**a**) (**b**)

Figure 2. Circuit diagram for the IPT system: (**a**) system structure diagram and (**b**) equivalent circuit diagram.

In Figure 2, U_{in} represents the DC input voltage, while U_t signifies the inverter output voltage. I_t and I_r denote the currents flowing through the transmitting and receiving coils, respectively. C_t stands for the compensation capacitor at the transmitter end, and C_r corresponds to the compensation capacitor at the receiver end. R_t is the internal resistance of the transmitting coil, and U_r indicates the rectifier input voltage. L_1, L_2, and L_n are the coil self-inductances for the first, second, and nth turn spacings, respectively, with the sum of the coil self-inductances of n turn spacings constituting the transmitting coil self-inductance. R_r refers to the internal resistance of the receiving coil, while L_r represents

the receiving coil self-inductance. M_{1r}, M_{2r}, and M_{nr} are the mutual inductances between the coil and the receiving coil for the first, second, and nth turn spacings, respectively. C_F is the filter capacitor of the rectifier circuit, R_L denotes the load resistance, U_O is the voltage across the load, and R_{eq} represents the equivalent load resistance.

According to Kirchhoff's law, we can derive:

$$\begin{cases} U_t = R_t I_t + j\left(\sum_{p=1}^{n} \omega L_p - 1/\omega C_t\right) I_t - \sum_{p=1}^{n} j\omega M_{pr} I_r \\ 0 = \left(R_r + R_{eq}\right) I_r + j(\omega L_r - 1/\omega C_r) I_r - \sum_{p=1}^{n} j\omega M_{pr} I_t \end{cases} \tag{1}$$

When the system reaches the resonant state, it meets the following equation:

$$\begin{cases} 1/\omega C_t = \sum_{p=1}^{n} \omega L_p \\ 1/\omega C_r = \omega L_r \end{cases} \tag{2}$$

The transmitting circuit current, denoted by I_t, is given as follows:

$$I_t = \frac{U_t\left(R_{eq} + R_r\right)}{\omega^2\left(\sum_{p=1}^{n} M_{pr}\right)^2 + \left(R_{eq} + R_r\right)R_t} \tag{3}$$

The receiving circuit current, denoted by I_r, is given as follows:

$$I_r = \frac{\sum_{p=1}^{n} j\omega M_{pr} U_t}{\omega^2\left(\sum_{p=1}^{n} M_{pr}\right)^2 + \left(R_{eq} + R_r\right)R_t} \tag{4}$$

From this, the system output power and transmission efficiency can be obtained as follows:

$$P_{out} = \left[\frac{\sum_{p=1}^{n} \omega M_{pr} U_t}{\omega^2\left(\sum_{p=1}^{n} M_{pr}\right)^2 + R_t\left(R_{eq} + R_r\right)^2}\right]^2 R_{eq} \tag{5}$$

$$\eta = \frac{R_{eq}\left(\sum_{p=1}^{n} \omega M_{pr}\right)^2}{R_t\left(R_{eq} + R_r\right)^2 + \left(R_{eq} + R_r\right)\left(\sum_{p=1}^{n} \omega M_{pr}\right)^2} \tag{6}$$

The influential relationship of the mutual inductance M_{tr} on the system output power and transmission efficiency is plotted as shown in Figure 3, based on Equations (5) and (6), which represent the superposition of mutual inductance between the transmitting coil and the receiving coil, that is, $M_{tr} = M_{1r} + M_{2r} + \ldots + M_{nr}$.

Figure 3 demonstrates that as the mutual inductance increases, the system output power initially rises and then declines. Concomitantly, the system transmission efficiency increases with the growth of mutual inductance, eventually reaching a plateau after surpassing a specific value. It is important to note that M_{tr} is linked to both the magnetic flux (ϕ) and the magnetic induction intensity (B). Therefore, through the design and optimization of

the magnetic coupling mechanism, achieving a uniform magnetic field is possible, leading to an enhancement in the system's transmission performance.

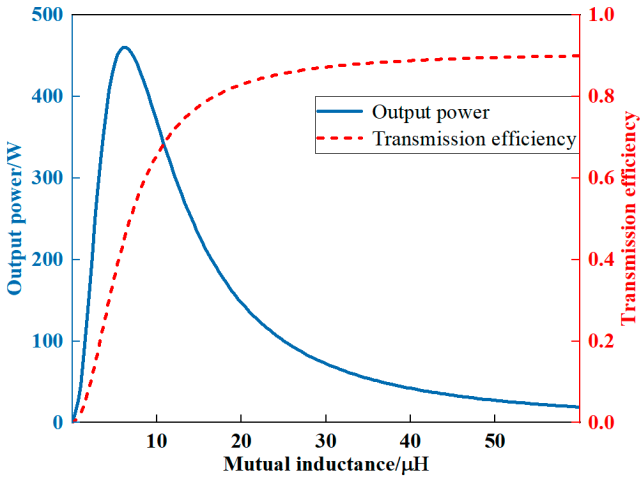


Figure 3. The relationship between output power, transmission efficiency, and mutual inductance.

3. Analysis of Magnetic Induction Distribution and Mutual Inductance Calculation for Combined Coils

3.1. Magnetic Induction Intensity Distribution of Combined Coils

The magnetic induction intensity distribution characteristics of both mosquito coils and close-wound coils were investigated by obtaining the magnetic field distribution on the receiving coil plane at varying heights (h) for these coil types via simulation, as shown in Figures 4 and 5.

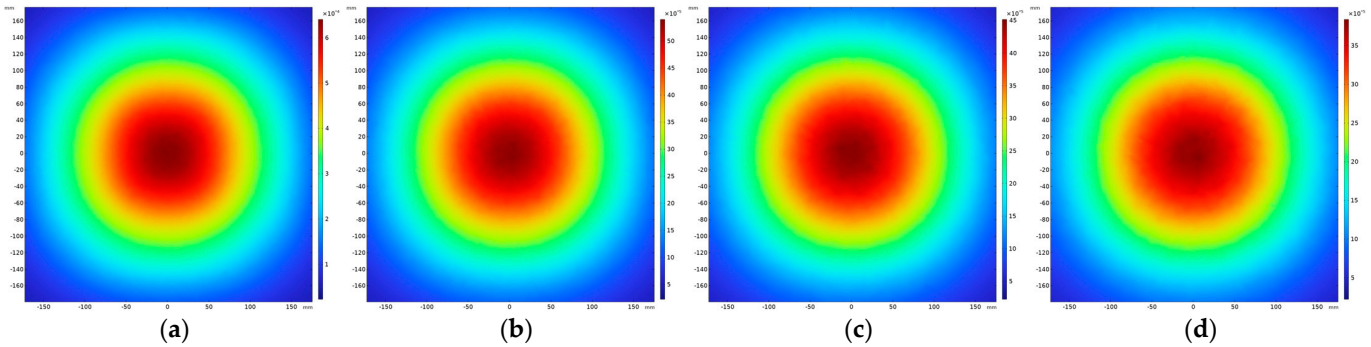


Figure 4. Magnetic flux density distributions of the mosquito coil: (**a**) h = 40 mm; (**b**) h = 50 mm; (**c**) h = 60 mm; and (**d**) h = 70 mm.

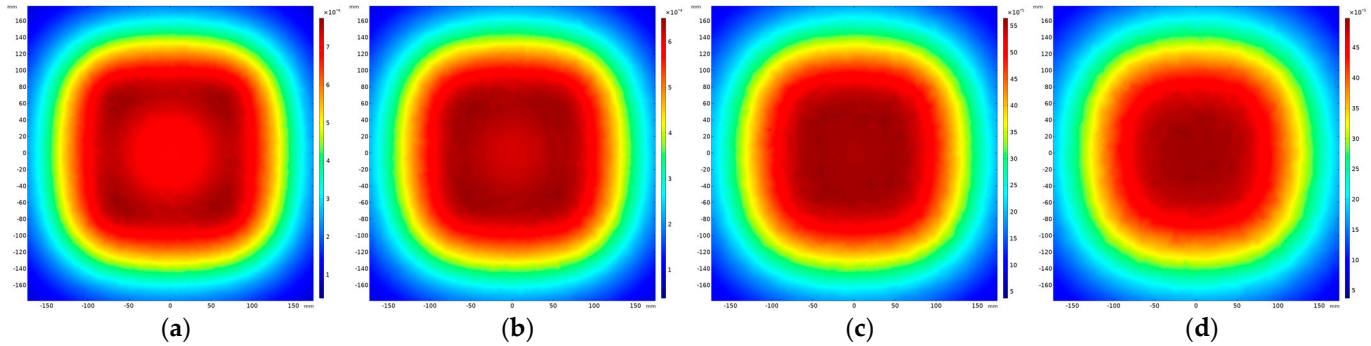


Figure 5. Magnetic flux density distributions of the close-wound coil: (**a**) h = 40 mm; (**b**) h = 50 mm; (**c**) h = 60 mm; and (**d**) h = 70 mm.

Using the center of the mosquito coil and close-wound coil as the origin, a straight line was drawn through the points (−150, 0, *h*) mm and (150, 0, *h*) mm. The normalized curve of the magnetic induction intensity along this line for different heights of the mosquito coil and close-wound coil is presented in Figure 6.

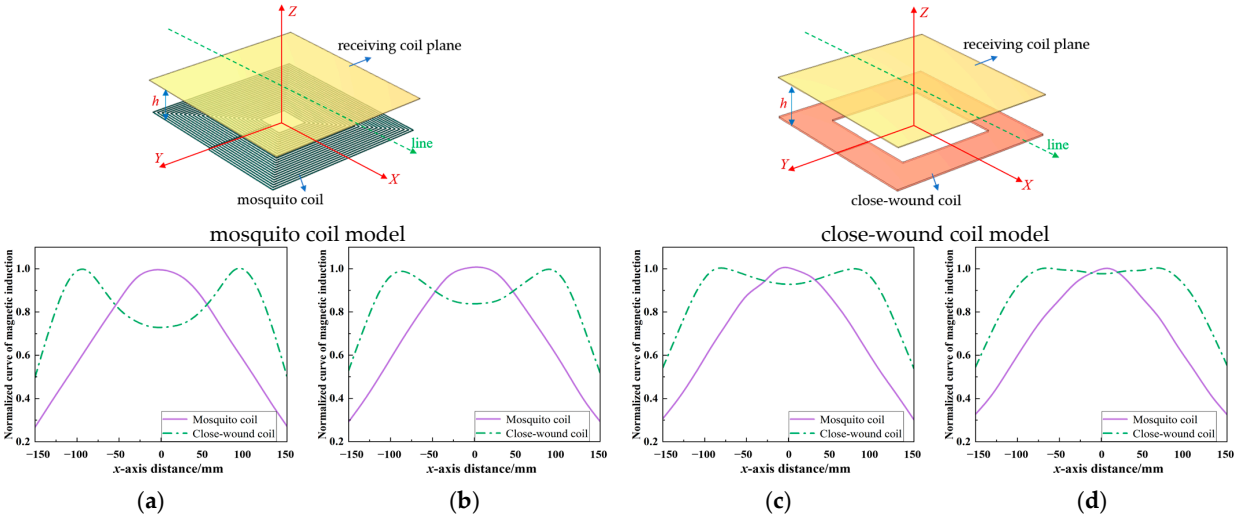


Figure 6. Normalized curves of magnetic induction intensity distributions of the coil on line: (**a**) *h* = 40 mm; (**b**) *h* = 50 mm; (**c**) *h* = 60 mm; and (**d**) *h* = 70 mm.

The magnetic induction intensity is most prominent in the central region of the mosquito coil, as depicted in Figures 4–6. The magnetic field gradually diminishes from the coil center outward. In contrast, the magnetic induction intensity is concentrated on both sides of the close-wound coil, resulting in a decrease in the magnetic field in the central area. This is evident from the comparative analysis of the two coil types as illustrated in the figures.

This paper proposes a combined coil that merges the characteristics of the mosquito coil and close-wound coil, with the center of the combined coil comprising the mosquito coil and the outer portion made up of the close-wound coil. The inner and outer coils are connected in the same direction to form a combined coil. This design aims to address the issues of a weak magnetic field on the outer part of the mosquito coil and a low magnetic field intensity at the center of the close-wound coil, ultimately achieving a more uniform magnetic field-intensity distribution based on the magnetic field distribution characteristics of both coil types.

3.2. Mutual Inductance Calculation of Combined Coils

A schematic diagram showing the horizontal misalignment of a single-turn square coil is depicted in Figure 7.

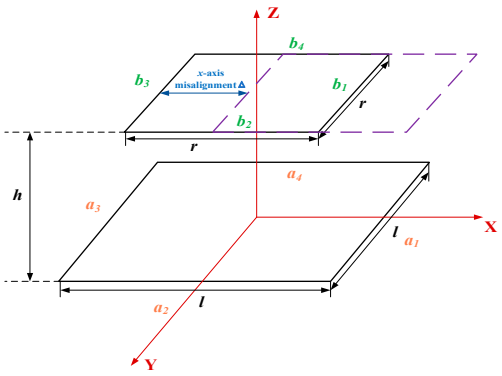


Figure 7. Schematic diagram of the horizontal misalignment of a single-turn square coil.

The transmitting coil and the receiving coil consist of two coaxially aligned coils. In this arrangement, h represents the distance between the transmitting and receiving coils, l is the side length of the transmitting coil, r is the side length of the receiving coil, and Δ is the distance the receiving coil shifts in the positive direction along the x-axis. The receiving coil's sides are labeled as b_1, b_2, b_3, and b_4, while the transmitting coil's four sides are a_1, a_2, a_3, and a_4. The mutual inductance M of the square coil can be considered as the superposition of the mutual inductance between two parallel sides [19]. This setup defines the key parameters and relationships essential for understanding the interaction between the transmitting and receiving coils.

$$M = M_{a_1b_1} + M_{a_1b_3} + M_{a_2b_2} + M_{a_2b_4} + M_{a_3b_3} + M_{a_3b_1} + M_{a_4b_4} + M_{a_4b_2} \tag{7}$$

After defining the coordinates of any point on sides a_1 and b_1 as $(l/2, y_1, 0)$ and $(r/2, y_2, h)$, respectively, and the coordinates of any point on sides a_2 and b_2 as $(x_1, l/2, 0)$ and $(x_2, r/2, h)$, respectively, the M_{a1b1} and M_{a2b2} values following a horizontal misalignment Δ undergone by the receiving coil can be determined in accordance with the Neumann formula as follows [20]:

$$M_{a_1b_1} = \frac{\mu_0}{4\pi} \int_{-\frac{r}{2}+\Delta}^{\frac{r}{2}+\Delta} \int_{-\frac{l}{2}}^{\frac{l}{2}} \frac{dy_1 dy_2}{\sqrt{\left(\frac{l-r}{2}\right)^2 + (y_1 - y_2)^2 + h^2}} \tag{8}$$

$$M_{a_2b_2} = \frac{\mu_0}{4\pi} \int_{-\frac{r}{2}}^{\frac{r}{2}} \int_{-\frac{l}{2}}^{\frac{l}{2}} \frac{dx_1 dx_2}{\sqrt{(x_1 - x_2)^2 + \left(\frac{l-r}{2} - \Delta\right)^2 + h^2}} \tag{9}$$

In the formula, μ_0 represents the magnetic permeability of a vacuum, where $\mu_0 = 4 \times 10^{-7}$.

Similarly, the M_{a1b3}, M_{a2b4}, M_{a3b3}, M_{a3b1}, M_{a4b4}, and M_{a4b2} can be obtainedfrom a horizontal misalignment Δ between the transmitting and receiving coils.

The M_{a1b1}, M_{a1b3}, M_{a2b2}, M_{a2b4}, M_{a3b3}, M_{a3b1}, M_{a4b4}, and M_{a4b2} can be obtained when the horizontal misalignment Δ is 0 and the transmitting coil and the receiving coil are aligned coaxially.

In light of Equations (8) and (9), the mutual inductance for the multi-turn mosquito coil can be derived under both alignment and misalignment scenarios. Here, we denote the number of turns of the mosquito coil as N_m and the coil turn spacing as d. Given that the turn spacing d of the mosquito coil is considerably larger than the diameter D of the single-turn coil, D can be disregarded when calculating the side length of the mosquito coil. Consequently, the side length for the N_m-th turn of the mosquito coil can be determined as follows:

$$l_{N_m} = l + 2d(N_m - 1) \tag{10}$$

By substituting Equation (10) into Equation (8), the M_{a1b1} of the N_m-th turn of the mosquito coil can be obtained as follows:

$$M_{a_1b_1(N_m)} = \frac{\mu_0}{4\pi} \int_{-\frac{r}{2}}^{\frac{r}{2}} \int_{-\frac{l_{N_m}}{2}}^{\frac{l_{N_m}}{2}} \frac{dx_1 dx_2}{\sqrt{(x_1 - x_2)^2 + \left(\frac{l_{N_m}-r}{2} - \Delta\right)^2 + h^2}} \tag{11}$$

The total $M_{a1b1(\text{total})}$ for N_m turns can be obtained as follows:

$$M_{a_1b_1(\text{total})} = \sum_{i=1}^{N_1} M_{a_1b_1(i)} \tag{12}$$

The mutual inductance M_{mr} between the multi-turn mosquito coil and the square coil comprising N_r turns can be expressed as follows:

$$\begin{aligned} M_{mr} = &\sum_{i=1}^{N_m}\sum_{j=1}^{N_r} M_{a_1(i)b_3(j)} + \sum_{i=1}^{N_m}\sum_{j=1}^{N_r} M_{a_1(i)b_1(j)} + \sum_{i=1}^{N_m}\sum_{j=1}^{N_r} M_{a_2(i)b_2(j)} + \sum_{i=1}^{N_m}\sum_{j=1}^{N_r} M_{a_2(i)b_4(j)} \\ &+ \sum_{i=1}^{N_m}\sum_{j=1}^{N_r} M_{a_3(i)b_3(j)} + \sum_{i=1}^{N_m}\sum_{j=1}^{N_r} M_{a_3(i)b_1(j)} + \sum_{i=1}^{N_m}\sum_{j=1}^{N_r} M_{a_4(i)b_2(j)} + \sum_{i=1}^{N_m}\sum_{j=1}^{N_r} M_{a_4(i)b_4(j)} \end{aligned} \tag{13}$$

The diameter of the single-turn coil is denoted by D, and the number of turns for the close-wound coil is denoted by N_c. Since the turn spacing d of the close-wound coil is approximately equal to 0, it can be disregarded when computing the side length of the close-wound coil. Thus, the side length for the N_c-th turn of the close-wound coil can be described as follows:

$$l_{N_c} = l + 2d(N_c - 1) \tag{14}$$

Similarly, drawing upon Equations (8) and (9), the $M_{a1b1(Nc)}$ for the N_c-th turn of the close-wound coil, the $M_{a1b1(Nc)}$ for the N_c-th turn following horizontal misalignment, and the mutual inductance M_{cr} between the multi-turn, close-wound coil and the square coil with N_r turns can be derived.

Therefore, the mutual inductance between the combined coil and the receiving coil can be represented as the superposition of the mutual inductances among the mosquito coil, close-wound coil, and receiving coil, respectively. The corresponding equation is given as follows:

$$M = \sum_{k=1}^{n_m} M_{(k)mr} + \sum_{p=1}^{n_c} M_{(p)cr} \tag{15}$$

In Equation (15), n_m denotes the total number of mosquito coils, k signifies the k-th mosquito coil counted from the innermost layer outward, n_c represents the overall quantity of close-wound coils, and p refers to the p-th close-wound coil counted from the innermost layer outward.

In conclusion, a relatively uniform magnetic induction intensity distribution can be achieved in the combined coil by the rational design of the quantity and coil parameters for both mosquito and close-wound coils. This design effectively reduces the fluctuations in mutual inductance during the misalignment process. Such an optimization strategy for coil design ensures a consistent magnetic induction intensity distribution, thereby enhancing the overall performance and stability of the combined coil system.

4. Optimization of Double-Mosquito Combination (DMC) Coils and Their Parameters

4.1. Design of Double-Mosquito Combination (DMC) Coils

The combined coil, as discussed in Section 3.1, is comprised of a mosquito coil at the center and a close-wound coil at the outer layer. This DMC coil exhibits three different turn spacings and can be arranged in two possible configurations: (1) with the first and third layers being mosquito coils, and the second layer being a close-wound coil; and (2) with the first and second layers as mosquito coils, and the third layer as a close-wound coil. The magnetic field distribution of the combined coil under these two conditions was simulated using COMSOL Multiphysics 5.6 software. As the turn spacing of the close-wound coil is approximately zero, the diameter D of the single-turn coil is used instead of its turn spacing. The turn spacing and width of each layer of the coil are denoted by d_1, W_1; d_2, W_2; and d_3, W_3, respectively. The specific parameters are detailed in Table 1, in which No.1 and No.2 share the same turn spacing and width, as do No.3 and No.4 as well as No.5 and No.6. No.1, No.3, and No.5 correspond to the first type of arrangement, while No.2, No.4, and No.6 correspond to the second type of arrangement.

Table 1. Parameters of mosquito coils and close-wound coils.

Parameters / Serial Number	d_1/mm	d_2/mm	d_3/mm	W_1/mm	W_2/mm	W_3/mm
1	15	2	12	45	36	36
2	15	12	2	45	36	36
3	18	2	15	54	40	45
4	18	15	2	54	45	40
5	16	12	2	48	36	40
6	16	2	12	48	40	36

Using the center of the combined coil as the origin, a straight line passing through the points (−150 mm, 0 mm, h mm) and (150 mm, 0 mm, h mm) is drawn. Figure 8 illustrates the distribution curve of the magnetic flux density along this line under different arrangement methods.

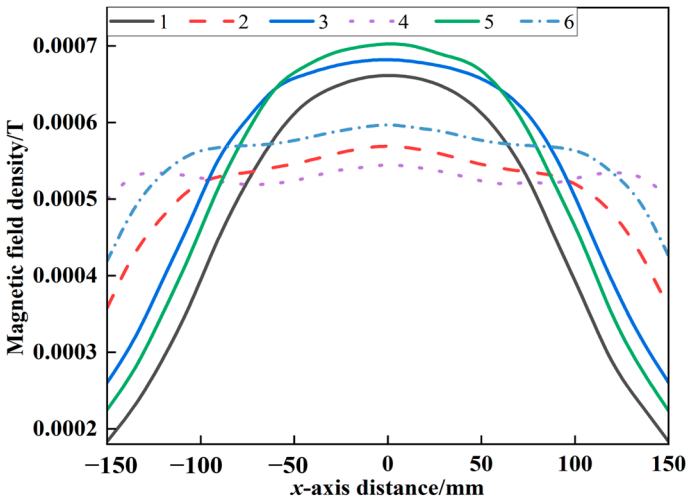


Figure 8. Normalized curve of magnetic induction intensity distribution on line.

As shown in Figure 8, the magnetic flux density distribution of the combined coil under the first arrangement method is high in the middle and low on both sides. The second arrangement method results in a more uniform distribution. Hence, to achieve a uniform magnetic flux density on the receiving coil plane of the combined coil, the second arrangement method is adopted, in which the turn spacing decreases gradually from the inside to the outside. The final schematic diagram of the DMC coil is illustrated in Figure 9.

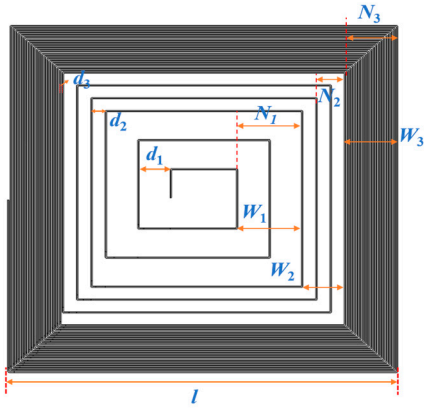


Figure 9. Coil based on double-mosquito combination (DMC) structure.

As shown in Figure 9, the first and second layers are mosquito coils, and the third layer is a close-wound coil. The inter-turn distances of the three layers of coils are denoted by d_1, d_2, and d_3, respectively. The widths of the three layers of coils are denoted by W_1, W_2, and W_3, respectively. The number of turns of the three layers of coils are denoted by N_1, N_2, and N_3, respectively. The total width of the coil is denoted by S.

In this paper, a DMC coil is fabricated using Litz wire with a single-turn coil diameter D of 2 mm. When the inter-turn spacing d of the coil is greater than D, the diameter of the Litz wire is negligible compared to its inter-turn spacing. Conversely, when d is less than or equal to D, the inter-turn spacing is negligible compared to the diameter of the Litz wire. Hence, the calculation formula for the DMC coil parameters is given by:

$$\begin{cases} W_1 = (N_1 - 1)d_1 \\ W_2 = (N_2 - 1)d_2 \\ W_3 = S - d_1 - W_1 - d_2 - W_2 - d_3 \\ N_3 = W_3/D \end{cases} \tag{16}$$

4.2. Optimization of Double-Mosquito Combination (DMC) Coil Parameters

The improved whale optimization algorithm (WOA) is used to optimize the parameters of the DMC coil. Given the total width S of the coil and the transmission distance h, the optimization determines the inter-turn distance d, width W, and number of turns N of the three-layer coil. This ensures a relatively uniform magnetic field distribution and a relatively stable mutual inductance for the DMC coil.

The whale optimization algorithm (WOA) is inspired by the hunting behavior of humpback whales in nature [21]. It has a simple and easy-to-implement principle, and it is widely applied to various optimization problems. In the WOA, the position of the optimal whale affects the position update of other whale individuals. To enhance the convergence speed and accuracy of the WOA, the beetle antennae search algorithm (BAS) [22] is employed to improve the position of the optimal whale. BAS searches on both sides of the optimal whale obtained using the WOA, in the domain of the side with a lower fitness value, calculates the new optimal whale position using the position update formula of the BAS, compares the optimal whale positions of the two algorithms, and selects the one with a lower fitness value as the leading whale.

Based on Equation (13), assuming that the total width of the coil S, the transmission distance h, and the horizontal misalignment distance Δ are constant, the objective function is the minimum mutual inductance fluctuation rate before and after the misalignment Δ, and the inter-turn spacing, width, and number of turns of the three-layer coil are the key parameters affecting the mutual inductance fluctuation rate. From Equation (15), d_1, d_2, N_1, and N_2 are known, and other coil parameters can be derived. Hence, the objective function of the DMC coil is:

$$\min f(x) = \frac{M - M_\Delta}{M} = f(d_1, d_2, N_1, N_2) \tag{17}$$

where M represents the mutual inductance of aligned coils, and M_Δ represents the mutual inductance after the coils are displaced.

S is the length of the outermost side of the coil, which is 300 mm. To prevent the DMC coil from exceeding S due to the large inter-turn distance of the first and second layer coils, the inter-turn distance of the first layer coil is limited to 25 mm or less. The inter-turn distance of the second layer coil is smaller than that of the first layer coil and is limited to 15 mm or less. To reduce the cost, the number of turns of the third layer coil is limited to 29 or less. The final optimization constraints for the coil parameters are:

$$s.t. \begin{cases} 20 \le d_1 \le 25 \\ 10 \le d_2 \le 15 \\ 1 \le N_1 \le (S/d_1) + 1 \\ 1 \le N_2 \le (S/d_2) + 1 \\ 1 \le N_3 \le 29 \end{cases} \tag{18}$$

The DMC coil parameter optimization process is illustrated in Figure 10.

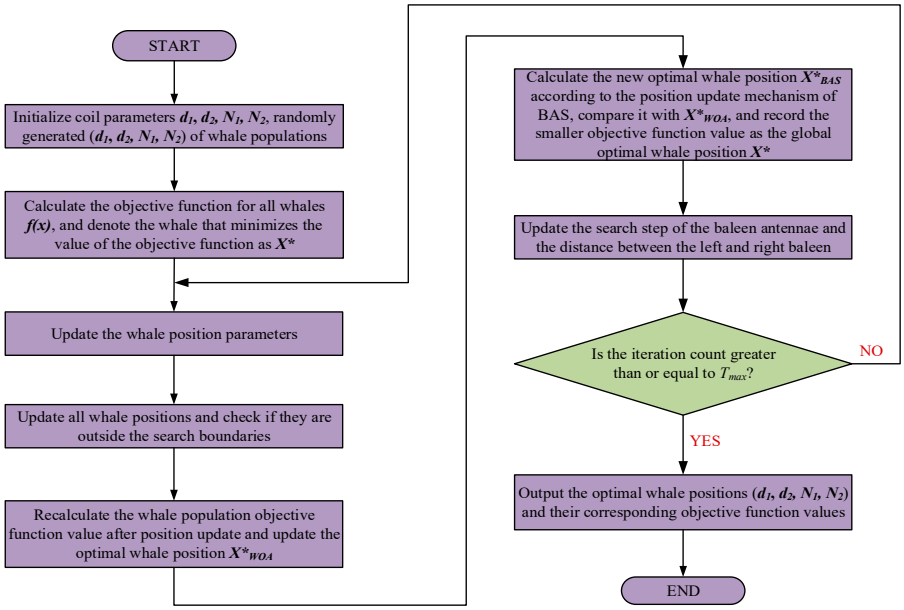


Figure 10. Flow chart for optimization of coil parameters.

The optimization steps are as follows:

- Initialize the DMC coil parameters (d_1, d_2, N_1, and N_2) and randomly generate a whale population (d_1, d_2, N_1, and N_2).
- Calculate the objective function $f(x)$ for each whale in the population, and mark the whale with the minimum objective function value as X^*.
- Update the position parameters of the whales and check whether they exceed the search boundary. If so, adjust them to the boundary value.
- Calculate the objective function value of the whales after the position update, and obtain the optimal whale position X^*_{WOA}.
- Based on the position update mechanism of the beetle antennae search algorithm (BAS), calculate the new optimal whale position X^*_{BAS}, and compare it with X^*_{WOA}. Choose the one with the lower objective function value as the global optimal whale position X^*.
- Update the beetle antennae parameters.
- If the number of iterations reaches or exceeds T_{max}, output the optimal whale position, which is the optimal solution (d_1, d_2, N_1, and N_2). Otherwise, update the whale position parameters and continue the process.

To verify the effectiveness of the improved algorithm, this paper compares the improved whale algorithm and WOA for parameter optimization. Figure 11 shows the comparison of the algorithm convergence results.

Figure 11 shows that the improved WOA and unimproved WOA have a similar convergence accuracy, but the improved WOA has a faster convergence speed and smaller objective function value. This implies that the beetle antennae search algorithm can effectively improve the WOA performance.

Table 2 shows the optimized coil parameters.

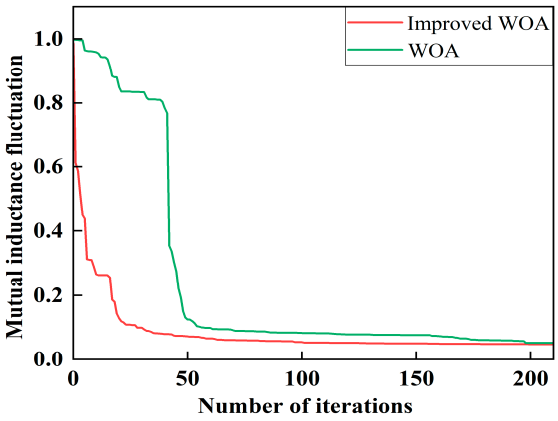


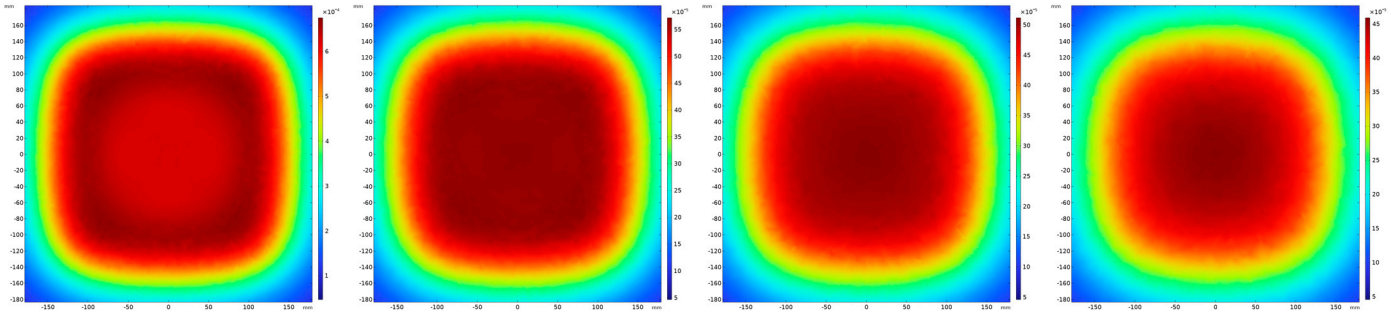
Figure 11. The iterative curve of optimization.

Table 2. DMC coil parameters.

Parameters / Layer Number	Turns Spacing *d*/mm	Width *W*/mm	Number of Turns *N*
First layer	25	50	3
Second layer	11	22	3
Third layer	2	40	20

4.3. Analyzing the Misalignment Features of the Optimized Double-Mosquito Combination (DMC) Coil

This paper studies the misalignment characteristics of the optimized DMC coil, using COMSOL Multiphysics to verify its uniform magnetic field distribution and small mutual inductance fluctuation. Figure 12 shows the distribution of the magnetic field intensity of the DMC coil (as the transmitting coil) on different height planes by changing the height h between the receiving coil and the transmitting coil.



(**a**) (**b**) (**c**) (**d**)

Figure 12. Magnetic flux density variation distribution of the DMC coil: (**a**) h = 40 mm; (**b**) h = 50 mm; (**c**) h = 60 mm; and (**d**) h = 70 mm.

As shown in Figure 12, the magnetic induction intensity of the DMC coil is approximately uniform within the square region of [−80 mm, 80 mm] for h = 40 mm and h = 70 mm, within the square region of [−100 mm, 100 mm] for h = 50 mm, and within the square region of [−90 mm, 90 mm] for h = 60 mm. Although the areas of approximately equal magnetic field strengths vary at different heights for the DMC coil, it is evident that the magnetic field fluctuates minimally over a wide range.

Figure 13 shows the law of mutual inductance change under the horizontal misalignment of the transmitting coil at different h values. The specific data are shown in Table 3.

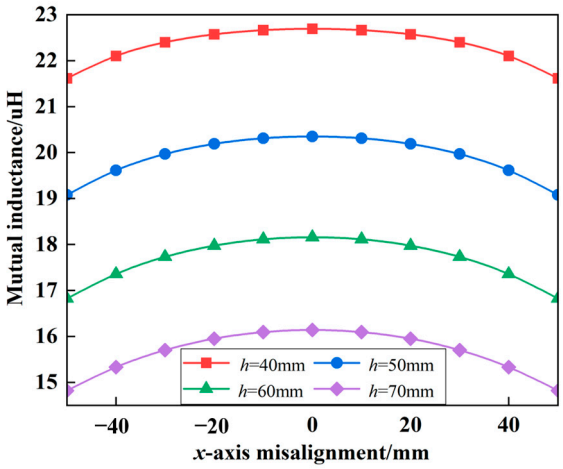


Figure 13. Mutual inductance variation patterns in the case of horizontal misalignment.

Table 3. Results of mutual sensing at different transmission distances.

Transmission Distance *h*/mm	*x*-Axis Misalignment/mm	Maximum Mutual Inductance/μH	Mutual Inductance Fluctuation Rate (%)
40	[−50, 50]	22.693	4.8
50	[−50, 50]	20.349	6.2
60	[−50, 50]	18.157	7.4
70	[−50, 50]	16.14	8.2

Based on Figure 13 and Table 3, the mutual inductance fluctuation of the DMC coil during the horizontal misalignment process is small for different transmission distances, and the maximum fluctuation rate is less than 8.2%. This demonstrates the excellent anti-misalignment performance of the DMC coil at different transmission distances.

5. Experimental Verification

An experimental platform based on the IPT system shown in Figure 2a was built, as depicted in Figure 14. The coupled coils and the receiving coil have an outer diameter of 142 mm × 142 mm, while the DMC coil, the mosquito coil, and the close-wound coil have an outer diameter of 300 mm × 300 mm. A was used as the controller in this experiment to collect the signals and generate the PWM waves. The transmitting and receiving coils of the magnetic coupling mechanism were wound with 0.1 mm × 200 strands of Litz wire. The coil mutual inductance was measured using a Chroma 11050-5M high-frequency LCR tester. The voltage at both ends of the load was measured using a Tektronix MSO 2024B oscilloscope, and the load current was measured using an RP1001C current probe.

The system input voltage was set to 45 V, the operating frequency f was 85 kHz, the self-inductance L_r of the receiving coil was 60.3 μH, the compensation capacitance C_r of the receiving coil was 58.2 nF, and the load R_L was 10 Ω. According to the actual coil parameters, the compensation circuit parameters were adjusted. The mutual inductances, system output voltages, output powers, and efficiencies of the three transmitting coils with the same receiving coil were compared. The self-inductance measurements of the three transmitting coils and the system compensation capacitance values are shown in Table 4.

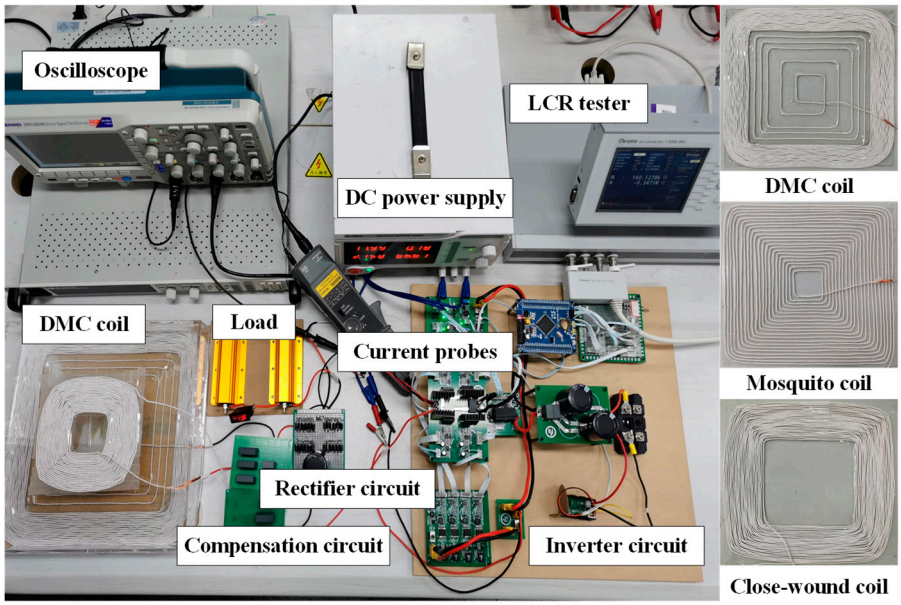


Figure 14. Experimental platform.

Table 4. Design values of system parameters.

Parameter / Coil Structure	Outer Diameter	Self-Inductance L_t	Compensating Capacitor C_t
DMC	300 mm	248.1 μH	14.1 nF
Mosquito coil	300 mm	75.2 μH	46.7 nF
Close-wound coil	300 mm	222.1 μH	15.8 nF

Using the position where the receiving coil and the transmitting coil are coaxially aligned and the transmission distance is 50 mm as the reference base, we measured the mutual inductance of the DMC, mosquito-coil, and close-wound coil transmitters during a 50mm horizontal misalignment of the receiving coil. The results are shown in Figure 15.

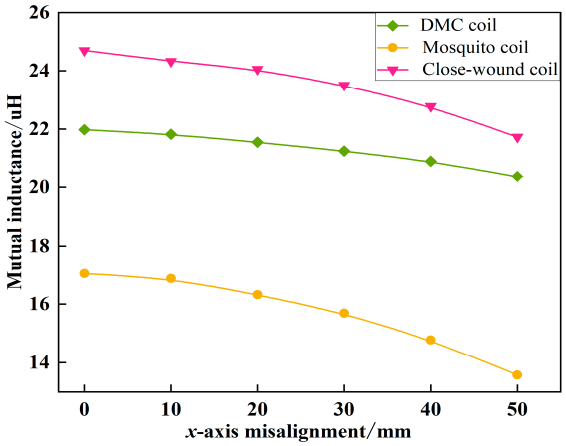


Figure 15. Mutual inductance of coils with misalignment in the horizontal plane.

Based on the experimental results, it can be observed that the mutual inductance fluctuation rate of the DMC and the receiving coil is 7.3% when the receiving coil undergoes a horizontal misalignment. This rate is significantly lower than the mutual inductance fluctuation rates of the close-wound coil (12%) and the mosquito coil (20.3%). Therefore, it can be concluded that the DMC coil is capable of ensuring the stable operation of the system under misalignment conditions.

The waveforms of the inverter output voltage U_t, inverter output current I_t, load terminal voltage U_l, and load current I_l for the DMC, mosquito, and close-wound coils are shown in Figure 16 under conditions of alignment with the receiving coil or horizontal misalignment.

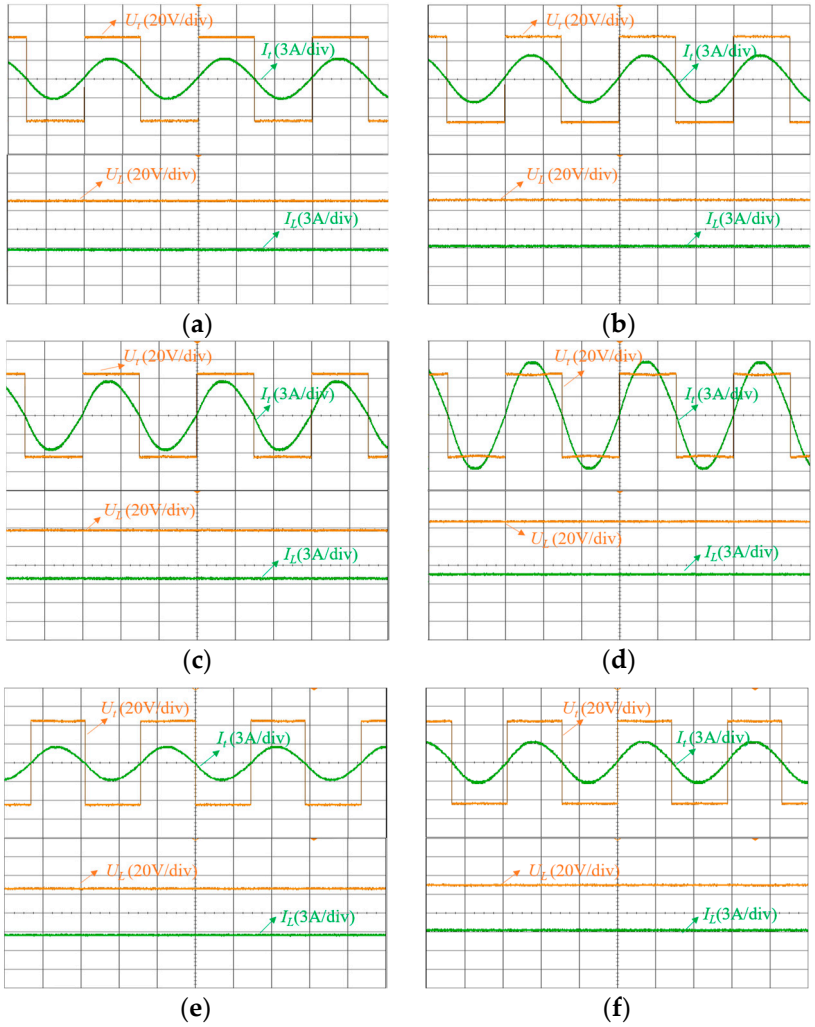


Figure 16. Waveforms of the system in two positions: (**a**) DMC coil, zero misalignment; (**b**) DMC coil, lateral misalignment; (**c**) mosquito coil, zero misalignment; (**d**) mosquito coil, lateral misalignment; (**e**) close-wound coil, zero misalignment; and (**f**) close-wound coil, lateral misalignment.

As shown in Figure 16, when R_L = 10 Ω, the output voltage of the IPT system with the DMC coil was 29.89 V and the efficiency was 83.3% when the coils were aligned; the output voltage was 32.09 V and the efficiency was 83.13% when the coils were displaced by 50 mm; the output voltage fluctuation rate of the system during the displacement process was 7.4%. The output voltage of the mosquito coil was 38.45 V, and the efficiency was 84.45% when the coils were aligned; the output voltage was 47.47 V, and the efficiency was 84.1% when the coils were displaced by 50 mm; the output voltage fluctuation rate of the system during the displacement process was 23.46%. The output voltage of the close-wound coil was 26.77 V, and the efficiency was 83.28% when the coils were aligned; the output voltage was 30.18 V, and the efficiency was 82.86% when the coils were displaced by 50 mm; the output voltage fluctuation rate of the system during the displacement process was 12.7%. It can be seen that the output voltage fluctuation rates of the three coils are significantly different, while the efficiencies are similar. Therefore, under the condition of comparable efficiency, the output voltage fluctuation rate is the main criterion for comparison. Compared with the mosquito coil and the close-wound coil, the output voltage fluctuation rate of the DMC coil is significantly lower, and the system's robustness to displacement is greatly improved.

To verify the strong anti-misalignment capability of the DMC coil under different load conditions, R_L was set to 20 Ω, 30 Ω, and 40 Ω respectively, and the transmission distance between the transmitting coil and the receiving coil was 50 mm. The output voltages and transmission efficiencies of the DMC, mosquito, and close-wound transmitting coils under different load conditions were measured when the receiving coil was horizontally misaligned by 50 mm relative to the transmitting coil, as shown in Figure 17.

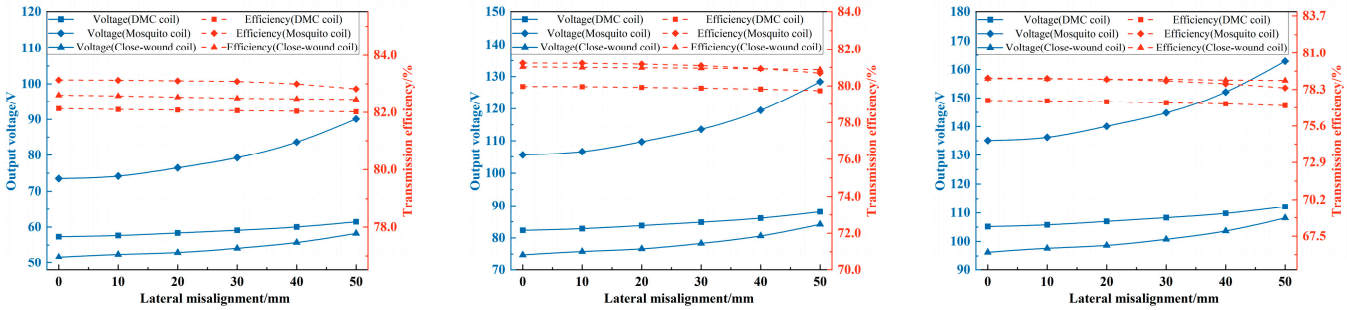
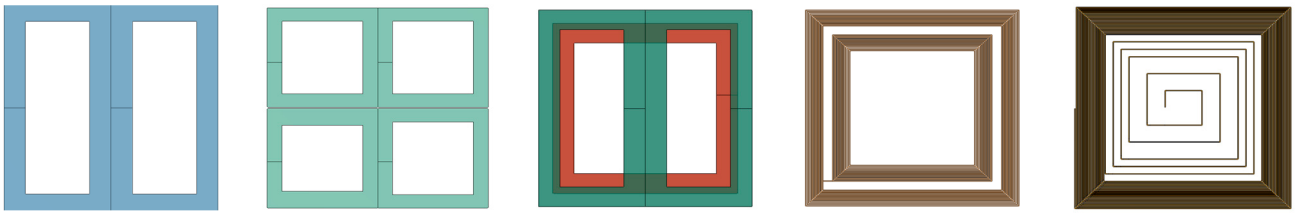


Figure 17. Plots of output voltages and transmission efficiencies with misalignments in the horizontal plane: (**a**) R_L = 20 Ω; (**b**) R_L = 30 Ω; (**c**) R_L = 40 Ω.

The experimental results show that when R_L was 20 Ω, 30 Ω, and 40 Ω respectively, the voltage fluctuation rates of the DMC coil during the horizontal misalignment process were 7.2%, 7%, and 6.7% respectively, and the transmission efficiencies after misalignment were 82.02%, 79.73%, and 77.11% respectively. The voltage fluctuation rates of the mosquito coil during the misalignment process were 22.5%, 21.6%, and 20.58% respectively, and the transmission efficiencies after misalignment were 82.82%, 80.69%, and 78.42% respectively. The voltage fluctuation rates of the close-wound coil during the misalignment process were 12.8%, 12.6%, and 12.42% respectively, and the transmission efficiencies after misalignment were 82.45%, 80.88%, and 78.99% respectively. The voltage fluctuations of DMC coils were significantly lower than those of mosquito-coil and close-wound coils at different loads. The transmission efficiencies of the DMC, mosquito coil, and close-wound coils were similar, with a difference of less than 1%, thus making the comparison of voltage fluctuation the main criterion for comparison, as the transmission efficiency was comparable. This demonstrated the outstanding robustness to displacement of DMC systems under different load conditions.

In addition, during the displacement process, the mutual inductance and the transmission efficiency decreased, but the output voltage increased. This phenomenon can be explained by referring to the theoretical curves of the output power, transmission efficiency, and mutual inductance shown in Figure 4. When the mutual inductance was in the right-side region of the mutual inductance value corresponding to the peak value of the output power, the displacement distance increased, the mutual inductance decreased, the output power first increased and then decreased, and the transmission efficiency decreased. Since the output power was proportional to the output voltage, when the displacement distance increased, the mutual inductance decreased, and the output voltage first increased and then decreased.

To demonstrate the advantages of the DMC coil proposed in this paper, it is compared with other coils in the literature. To ensure a consistent comparison, the outer diameter of the transmitting coil was set to be the same, and the receiving coil was the same closely wound coil. The coil structure schematic is shown in Figure 18. During the process of the receiving coil horizontally misaligning by 50 mm relative to the transmitting coil, the robustness to displacement of the IPT system with different transmitting coils was measured, as shown in Table 5.



(**a**) (**b**) (**c**) (**d**) (**e**)

Figure 18. Coil structure schematic: (**a**) DD; (**b**) QD; (**c**) DDQ; (**d**) reference [15]; and (**e**) this paper.

Table 5. Comparison of misalignment resistance in DMC systems.

Coil Structure	Outer Diameter (mm)	Number of Turns	Mutual Inductance Fluctuation Rate (%)	Output Voltage Fluctuation Rate (%)	Output Power Fluctuation Rate (%)	Transmission Efficiency (%)
DD	300	N_D* = 15	12	11.8	22.2	80
QD	300	N_D* = 15	9.3	9.1	17.3	82
DDQ	300	N_D* = 15	14.3	14.4	26.6	75
[15]	300	26	14.1	13.6	25.3	83
This paper	300	26	7.3	7	13.2	83.3

N_D* represents the turns in a single D coil.

As can be seen from the Table 5, under the same horizontal misalignment distance, the mutual inductance, output voltage, and output power fluctuation rates of the DMC coil proposed in this paper were all the smallest during the misalignment process. Compared with the existing coils, the coil proposed in this paper exhibited a better resistance to the misalignment distance, thereby ensuring that an IPT system with this coil can work efficiently and stably when the coupling mechanism is misaligned.

6. Conclusions

This paper proposes a DMC coil, which combines the magnetic field distribution characteristics of a mosquito coil and a close-wound coil to address the high anti-misalignment performance problem of the IPT system. From the perspective of coil structure optimization and enhancing the uniformity of magnetic field distribution, the coil aims to achieve a relatively even magnetic field distribution and minimize the fluctuations in system mutual inductance and output power. In this study, an equivalent circuit model of the IPT system is employed to derive analytical expressions for the system's transmission power and efficiency with respect to mutual inductance. Furthermore, the paper investigates the interaction between DMC coil parameters and mutual inductance. To optimize the DMC coil parameters, we propose an improved whale optimization algorithm, which incorporates the beetle antennae search algorithm. This improved algorithm is anticipated to yield more effective optimization results for the DMC coil design. This study involves a 3D simulation of the DMC coil and an investigation into its misalignment characteristics. To assess its anti-misalignment capability in comparison to other coil types, we established an experimental platform with a transmission distance of 50 mm. The experimental results reveal that the mutual inductance fluctuation rate of the DMC coil during the misalignment process is 13% lower than that of the mosquito coil and 4.7% lower than that of the close-wound coil with the same load and misalignment distance. Similarly, the output voltage fluctuation rate of the DMC coil is 16.06% lower than that of the mosquito coil and 5.3% lower than that of the close-wound coil. These findings illustrate a substantial decrease in both the mutual inductance and output voltage fluctuation rates of the DMC coil compared to other coil types. This suggests that an IPT system featuring the DMC coil can effectively provide stable power to an AGV even when there is a misalignment in the coupling coil. Based on this, to further enhance the coupling between the coils, ferrite cores can be added, and the

impact of factors such as core layout and core material on the mutual inductance between the coils can be comprehensively considered in order to further refine the analysis model of the coupling mechanism and lay a theoretical foundation for the global optimization of the IPT system.

Author Contributions: Conceptualization, W.H. and J.H.; methodology, J.H.; software, Y.H. and J.H.; validation, J.H., Y.H. and Y.Z.; formal analysis, W.H. and J.H.; investigation, Y.C. and Y.Z.; resources, Y.C. and Y.Z.; writing—original draft preparation, J.H.; writing—review and editing, W.H. and J.H.; visualization, J.H.; supervision, Y.C. All authors have read and agreed to the published version of the manuscript.

Funding: This research was funded by the National Natural Science Foundation of China under the grant number 61903129 and the Hubei University of Technology Doctoral Research Project under the grant number BSQD2020012.

Data Availability Statement: Data are contained within the article.

Conflicts of Interest: The authors declare no conflicts of interest.

References

1. Domajnko, J.; Prosen, N. A Wireless Power Transfer System Using a Double DD Quadrature Coil Structure. *Electronics* **2023**, *12*, 890. [CrossRef]
2. Zhang, X.; Liu, F.; Mei, T. Multifrequency phase-shifted control for multiphase multiload MCR WPT system to achieve targeted power distribution and high misalignment tolerance. *IEEE Trans. Power Electron.* **2021**, *36*, 991–1003. [CrossRef]
3. Mai, J.W.; Zeng, X.R.; Liu, Z.G. An IPT system based on S/SP compensation topology with high misalignment tolerance. *Proc. Chin. Soc. Electr. Eng.* **2023**, *43*, 1525–1537. [CrossRef]
4. Zhou, W.; Lan, J.H.; Mai, R.K. Research on power management strategy of DC microgrid with photovoltaic, energy storage and EV-wireless power transfer in V2G mode. *Trans. China Electrotech. Soc.* **2022**, *37*, 82–91. [CrossRef]
5. Kan, T.Z.; Mai, R.K.; Mercier, P.P. Design and analysis of a three-phase wireless charging system for lightweight autonomous underwater vehicles. *IEEE Trans. Power Electron.* **2018**, *33*, 6622–6632. [CrossRef]
6. Pan, S.S.; Mai, R.K.; Xu, Y.F. Three dimensional target space magnetic leakage shielding for AGV inductive charging system. *Trans. China Electrotech. Soc.* **2022**, *37*, 1078–1087. [CrossRef]
7. Lee, E.S.; Han, S.H. 2-D Thin Coil Designs of IPT for Wireless Charging of Automated Guided Vehicles. *IEEE J. Emerg. Sel. Top. Power Electron.* **2022**, *10*, 2629–2644. [CrossRef]
8. Saranya, N.; Kesavamurthy, T. Review on next generation wireless power transmission technology for implantable biomedical devices. *Int. J. Biomed. Eng. Technol.* **2021**, *35*, 207–222. [CrossRef]
9. Xiao, H.H.; Zhou, Q.S.; Xiong, S.X. Wireless power transfer system based on double-layer quadrature Double-D coupling structure with anti-misalignment and anti-deflection. *Trans. China Electrotech. Soc.* **2022**, *37*, 4004–4018. [CrossRef]
10. Solouma, N.H.; Kassahun, H.B.; Alsharafi, A.S.; Syed, A.; Gardner, M.R.; Alsharafi, S.S. An Efficient Design of Inductive Transmitter and Receiver Coils for Wireless Power Transmission. *Electronics* **2023**, *12*, 564. [CrossRef]
11. Li, Z.Q.; Li, S.Y.; Li, J. Mutual inductance calculation and optimization of multi receiver positive and negative series coil structure in dynamic wireless power transfer systems. *Trans. China Electrotech. Soc.* **2021**, *36*, 5153–5164. [CrossRef]
12. Zhang, P.; Saeedifard, M.; Onar, O.C. A field enhancement integration design featuring misalignment tolerance for wireless EV charging using LCL topology. *IEEE Trans. Power Electron.* **2021**, *36*, 3852–3867. [CrossRef]
13. Wang, S.; Hu, Z.; Rong, C. Planar multiple-antiparallel square transmitter for position-insensitive wireless power transfer. *IEEE Antennas Wirel. Propag. Lett.* **2017**, *17*, 188–192. [CrossRef]
14. Chen, Y.; Mai, R.; Zhang, Y. Improving misalignment tolerance for IPT system using a third-coil. *IEEE Trans. Power Electron.* **2019**, *34*, 3009–3013. [CrossRef]
15. Tan, R.X. Optimization Design of EV-WPT Magnetic Coupling Mechanism Offset Characteristics. Master's Thesis, Chongqing University, Chongqing, China, 2018.
16. Tan, P.G.; Xu, W.H.; Shang, G.X. Mutual inductance modeling and parameter optimization of wireless power transfer system with combined series-wound hexagonal coils. *Trans. China Electrotech. Soc.* **2023**, *38*, 2299–2309. [CrossRef]
17. Zhou, Y.Q.; Qiu, M.H.; Wang, Q.B.; Ma, Z.N.; Sun, H.; Zhang, X.Y. Research on Double LCC Compensation Network for Multi-Resonant Point Switching in Underwater Wireless Power Transfer System. *Electronics* **2023**, *12*, 2798. [CrossRef]
18. Wang, X.; Xu, J.; Ma, H.; Yang, P. A high efficiency LCC-S compensated WPT system with dual decoupled receive coils and cascaded PWM regulator. *IEEE Trans. Circuits Syst. II Express Briefs* **2020**, *67*, 3142–3146. [CrossRef]
19. Chen, Z.; Jing, W.W.; Huang, X.L. A promoted design for primary coil in roadway-powered system. *IEEE Trans. Magn.* **2015**, *51*, 8402004. [CrossRef]
20. Liu, F.X.; Yang, Y.; Jiang, D. Modeling and optimization of magnetically coupled resonant wireless power transfer system with varying spatial scales. *IEEE Trans. Power Electron.* **2017**, *32*, 3240–3250. [CrossRef]

21. Mirjalili, S.; Lewis, A. The whale optimization algorithm. *Adv. Eng. Softw.* **2016**, *95*, 51–67. [CrossRef]
22. Jiang, X.; Li, S. BAS: Beetle antennae search algorithm for optimization problems. *arXvi* **2017**, arXiv:1710.10724. [CrossRef]

Disclaimer/Publisher's Note: The statements, opinions and data contained in all publications are solely those of the individual author(s) and contributor(s) and not of MDPI and/or the editor(s). MDPI and/or the editor(s) disclaim responsibility for any injury to people or property resulting from any ideas, methods, instructions or products referred to in the content.